

LPO with a [100] density maximum close to lineation indicates preferred alignment of (100) and hence subgrain boundaries normal to lineation. This has an important implication for the generation of deep-focus earthquakes, which are possibly triggered by transformation of olivine to high-pressure phases^{19–24}. In a descending slab, the phase transformation of olivine to β -phase (wadsleyite) and γ -phase (ringwoodite) would occur first at regions of high Fe concentrations, because Fe-rich olivine transforms at a lower pressure than Mg-rich olivine at the same temperatures^{25,26}. Moreover, stacking faults along which the crystal lattice is transformed to ringwoodite are preferentially formed parallel to (100) in olivine^{27,28}. Thus the phase transformation would preferentially occur parallel to (100) in olivine, which is preferentially aligned normal to lineation, that is, in planar arrays. The high-pressure phases thus formed are much finer-grained than the host olivine^{21,23,24}, and possibly deform superplastically by a grain-size-sensitive flow—in contrast to the host olivine plastically deforming by grain-size-insensitive dislocation creep. The formation of high-pressure phases in planar arrays may therefore lead to shear instability in descending slabs, and trigger deep-focus earthquakes in these slabs.

Orowan's equation indicates that strain rate is proportional to dislocation velocity²⁹. The observed Fe zoning in naturally deformed olivine implies the moving of dislocations at speeds slow enough to drag a Cottrell atmosphere, probably because of very low strain rates ($\sim 10^{-14} \text{ s}^{-1}$) in the mantle. If the strain rate is much higher, as in deformation experiments (generally $\geq 10^{-6} \text{ s}^{-1}$), fast-moving dislocations would leave the Cottrell atmosphere behind, resulting in no Fe concentrations along dislocations. The presence of a Cottrell atmosphere also has a pinning effect on dislocations and inhibits their movement. Accordingly, flow laws at high and low strain-rate conditions are different³⁰. Hence the plasticity of olivine at very low strain rates in the mantle may be different from that at the high strain rates achieved in the laboratory—this needs to be explored in the future, to obtain a better understanding of the dynamics of the Earth's interior. □

Received 23 August; accepted 6 November 2001.

1. Li, J. C. M., Nolfi, F. V. Jr & Johnson, C. A. Diffusional equilibrium of substitutional atoms in a stressed solid. *Acta Metall.* **19**, 749–752 (1971).
2. Green, H. W. II On the thermodynamics of non-hydrostatically stressed solids. *Phil. Mag.* **41**, 637–647 (1980).
3. Kitamura, M., Matsuda, H. & Morimoto, N. Direct observation of the Cottrell atmosphere in olivine. *Proc. Jpn Acad.* **62**, 149–152 (1986).
4. Dimos, D., Wolfenstine, J. & Kohlstedt, D. L. Kinetic demixing and decomposition of multi-component oxides due to a nonhydrostatic stress. *Acta Metall.* **36**, 1543–1552 (1988).
5. Ozawa, K. Stress-induced Al–Cr zoning of spinel in deformed peridotites. *Nature* **338**, 141–144 (1989).
6. Cottrell, A. H. in *Report of the Strength of Solids* 30–36 (The Physical Society, London, 1948).
7. Blavette, D., Cadel, E., Fraczkiewicz, A. & Menand, A. Three-dimensional atomic-scale imaging of impurity segregation to line defects. *Science* **286**, 2317–2319 (1999).
8. Ben Ismail, W. & Mainprice, D. An olivine fabric database: An overview of upper mantle fabrics and seismic anisotropy. *Tectonophysics* **296**, 145–157 (1998).
9. Kohlstedt, D. L., Goetze, C., Durham, W. B. & Vandersande, J. B. New technique for decorating dislocations in olivine. *Science* **19**, 1045–1091 (1976).
10. Karato, S. Scanning electron microscope observation of dislocations in olivine. *Phys. Chem. Minerals* **14**, 245–248 (1986).
11. Ozawa, K. Partitioning of elements between constituents minerals in peridotites from the Miyamori ultramafic complex, Kitakami Mountains, Northeast Japan: Estimation of P–T condition and igneous composition of minerals. *J. Fac. Sci. Univ. Tokyo II* **21**, 115–137 (1986).
12. Kawasaki, T. & Ito, E. An experimental determination of the exchange of Fe^{2+} and Mg^{2+} between olivine and Ca-rich clinopyroxene. *Am. Mineral.* **79**, 461–477 (1994).
13. McGuire, A. V., Dyar, M. D. & Nielson, J. E. Metasomatic oxidation of upper mantle peridotite. *Contrib. Mineral. Petrol.* **109**, 252–264 (1991).
14. Banfield, J. F., Dyar, M. D. & McGuire, A. V. The defect microstructure of oxidized mantle olivine from Dish Hill, California. *Am. Mineral.* **77**, 977–986 (1992).
15. Carter, N. L. & Ave Lallemand, H. G. High temperature flow of dunite and peridotite. *Geol. Soc. Am. Bull.* **81**, 2181–2202 (1970).
16. Furusho, M. & Kanagawa, K. Transformation-induced strain localization in a lherzolite mylonite from the Hidaka metamorphic belt of central Hokkaido, Japan. *Tectonophysics* **313**, 411–432 (1999).
17. Ito, E. & Sato, H. in *High-Pressure Research: Application to Earth and Planetary Sciences* (eds Syono, Y. & Manghni, H.) 257–262 (Terrapub/American Geophysical Union, Tokyo/Washington DC, 1992).
18. Iidaka, T. & Furukawa, Y. Double seismic zone for deep earthquakes in the Izu-Bonin subduction zone. *Science* **263**, 1116–1118 (1994).
19. Kirby, S. H., Stein, S., Okal, E. A. & Rubie, D. C. Metastable mantle phase transformations and deep earthquakes in subducting oceanic lithosphere. *Rev. Geophys.* **34**, 261–306 (1996).

20. Kirby, S. H. Localized polymorphic phase transformations in high-pressure faults and applications to the physical mechanism of deep earthquakes. *J. Geophys. Res.* **92**, 13789–13800 (1987).
21. Green, H. W. II & Burnley, P. C. A new self-organizing mechanism for deep-focus earthquakes. *Nature* **341**, 733–737 (1989).
22. Kirby, S., Durham, W. B. & Stern, L. A. Mantle phase changes and deep-earthquake faulting in subducting lithosphere. *Science* **252**, 216–225 (1991).
23. Burnley, P. C., Green, H. W. II & Prior, D. J. Faulting associated with the olivine to spinel transformation in Mg_2GeO_4 and its implications for deep focus earthquakes. *J. Geophys. Res.* **96**, 425–443 (1991).
24. Tingle, T. N., Green, H. W. II, Scholtz, C. H. & Kocynski, T. A. The rheology of faults triggered by the olivine–spinel transformation in Mg_2GeO_4 and its implications for the mechanism of deep focus earthquakes. *J. Struct. Geol.* **15**, 1249–1256 (1993).
25. Katsura, T. & Ito, E. The system $\text{Mg}_2\text{SiO}_4 - \text{Fe}_2\text{SiO}_4$ at high pressure and temperatures: precise determination of stabilities of olivine, modified spinel, and spinel. *J. Geophys. Res.* **94**, 15663–15670 (1989).
26. Akaogi, M., Ito, E. & Navrotsky, A. Olivine-modified spinel-spinel transitions in the system $\text{Mg}_2\text{SiO}_4 - \text{Fe}_2\text{SiO}_4$: calorimetric measurements, thermochemical calculation, and geophysical. *J. Geophys. Res.* **94**, 15671–15685 (1989).
27. Poirier, J.-P. in *Anelasticity in the Earth* (eds Stacey, F. D., Paterson, M. S. & Nicholas, A.) 113–117 (American Geophysical Union and Geological Society of America, Washington DC/Boulder, 1981).
28. Kerschhofer, L., Rubie, D. C., Sharp, T. G., McConnell, J. D. C. & Dupas-Bruzek, C. Kinetics of intracrystalline olivine–ringwoodite transformation. *Phys. Earth Planet. Inter.* **121**, 59–76 (2000).
29. Poirier, J.-P. in *Creep of Crystals* 62–63 (Cambridge Univ. Press, Cambridge, 1985).
30. Yoshinaga, H. in *Rheology of Solids and of the Earth* (eds Karato, S. & Toriumi, M.) 29–41 (Oxford Science Publications, New York, 1989).

Acknowledgements

We thank K. Ozawa for critical reading of the manuscript, H. Ishisako for making thin sections, Y. Takahashi for his contribution to the XANES study at the KEK photon factory in Tsukuba, Japan, and N. Abe for supplying the specimens from the southern Alps. This study was supported by JSPS (J.A.).

Competing interests statement

The authors declare that they have no competing financial interests.

Correspondence and requests for materials should be addressed to J.A. (e-mail: ando@letitbe.geol.sci.hiroshima-u.ac.jp).

.....
Horses damp the spring in their step

Alan M. Wilson*, M. Polly McGuigan*, Anne Su† & Anton J. van den Bogert†

* *Department of Veterinary Basic Sciences, The Royal Veterinary College, Hatfield, Herts AL9 7TA, UK*

† *Department of Biomedical Engineering, Cleveland Clinic Foundation, 9500 Euclid Avenue, Cleveland, Ohio 44195, USA*

.....
The muscular work of galloping in horses is halved by storing and returning elastic strain energy in spring-like muscle–tendon units^{1,2}. These make the legs act like a child's pogo stick that is tuned to stretch and recoil at 2.5 strides per second. This mechanism is optimized by unique musculoskeletal adaptations: the digital flexor muscles have extremely short fibres and significant passive properties, whereas the tendons are very long and span several joints^{3,4}. Length change occurs by a stretching of the spring-like digital flexor tendons rather than through energetically expensive length changes in the muscle⁵. Despite being apparently redundant for such a mechanism⁵, the muscle fibres in the digital flexors are well developed. Here we show that the mechanical arrangement of the elastic leg permits it to vibrate at a higher frequency of 30–40 Hz that could cause fatigue damage to tendon and bone. Furthermore, we show that the digital flexor muscles have minimal ability to contribute to or regulate significantly the 2.5-Hz cycle of movement, but are ideally arranged to damp these high-frequency oscillations in the limb.

In a 500-kg horse, about 1,000 J of elastic energy are stored in the digital flexor tendons and suspensory ligament (interosseus muscle) of each leg in each stride^{2,6}. This is achieved by gravitational and

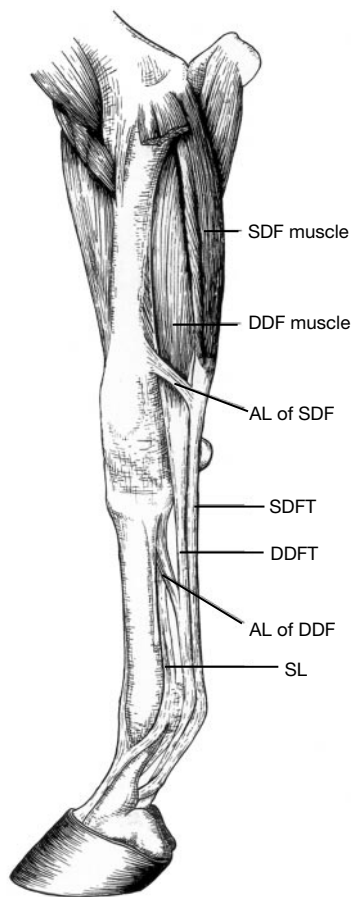


Figure 1 Equine distal forelimb (medial view) showing segments below the elbow, and the tendons and muscles that resist compression of the limb by the effect of gravitational and inertial forces during the stance phase of locomotion. This part of the limb is about 1 m long in a 450-kg thoroughbred racehorse. AL, accessory ligament; DDF, deep digital flexor; SDF, superficial digital flexor.

inertial forces that extend the metacarpophalangeal joint and stretch these collagenous structures (Fig. 1). Animals (including humans) that store elastic energy in their tendons have compliant tendons⁵ and minimize length change in the associated muscle^{7–9}. The muscle instead preloads^{10,11} and/or powers the system by shortening at low tendon forces⁷. Further efficiency gains may be achieved by shortening or removing the muscle fibres, because the energetic cost of generating isometric force is a function of muscle fibre length over activated volume^{3–5}. The endpoint of this optimization is shown in the completely collagenous interosseus muscle of the adult horse.

However, the equine forelimb superficial and deep digital flexor muscles remain well developed (mass 600–1,000 g), and 98% (see Methods) of the physiological cross-sectional area comprises extremely short (superficial, 2–6 mm; deep, 6–17 mm) muscle fibres^{1,6,10,11}. Similar short-fibred muscles exist in the hindlimb. Each muscle has a maximum isometric force of about 5,000 N ($n = 5$). The tendons are about 700 mm long and the muscles about 400 mm long. A peak tendon strain of 8–12% during locomotion^{1,12,13} equates to a tendon elongation of 70 mm and, assuming similar aponeurosis strains, a muscle elongation of 40 mm. Both muscles are protected from overextension by short (50 mm) and hence, when loaded, stiff accessory ligaments that link the tendon distal to the muscle belly to the bone, effectively acting as an additional parallel elastic element.

Assuming a change in sarcomere length of 35% and muscle force in excess of the long-fibred head isometric capacity (230 N), then

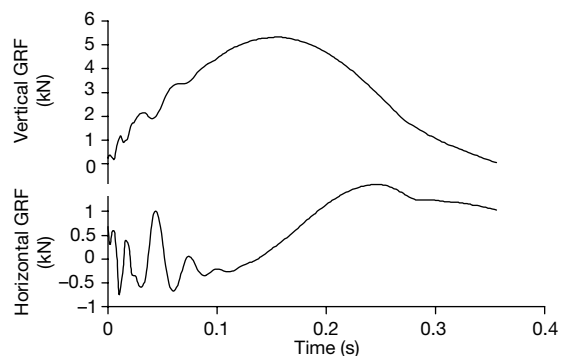


Figure 2 Plot of horizontal (in direction of locomotion) and vertical limb ground reaction force (GRF) against time for a 450-kg horse trotting at 3 m s^{-1} over a 6-mm-thick polyester/rubber-matting-covered conveyor-belt force plate. The inflections in the curves during early stance are due to limb vibration excited by foot impact.

the superficial and deep digital flexor muscle contractile elements should change length by only 1–2 mm and 2–6 mm, respectively. The long-fibred head appears sufficient to flex the digit during limb protraction, but the role of the short-fibred heads remains unclear. With potential contractile element length changes of 2 and 6 mm in a muscle tendon unit elongation of 60–80 mm, the muscles appear inappropriate for tuning the leg spring¹⁰ or driving the spring system as in other energy-storing tendons^{7–9}. It is possible, however, that the short fibres can, owing to lateral force transmission through the complex three-dimensional (3D) architecture of the muscle, achieve a length change greater than that predicted from fibre-length measurements¹⁴.

Hoof impact, slide and resonance lasts 20–30 ms. Foot impact excites the equine limb to vibrate in a cranio-caudal direction at a frequency of 30–40 Hz (Fig. 2)¹⁵. The vibrations are similar on different surfaces (tarmac $35.9 \pm 1.2 \text{ Hz}$; concrete $35.8 \pm 2.1 \text{ Hz}$; rubber matting $34.9 \pm 1.2 \text{ Hz}$; $n = 8$), and correspond to a muscle–tendon unit length change of about 2 mm (from joint angle changes) and an energy of 4–8 J. The vibrations are damped within 100 ms on hard surfaces and more quickly on soft surfaces. Similar frequency oscillations occur in the hindlimb and a simulation thereof⁶, but are damped within a cycle. Notably, 40–50-Hz horizontal vibrations are present for about 100 ms after impact in accelerometer and kinematic data recorded from the human tibia during barefoot running¹⁷.

Excessive high-frequency vibration in the limb will cause fatigue damage in both bone¹⁸ and tendon¹⁹ by increasing the number of loading cycles and the loading rate experienced by the distal limb tissues. Musculoskeletal injuries are extremely common in athletic horses, and most of them occur in this spring system, which has been shown to fail through cyclical fatigue damage in as little as 10,000 strides of gallop^{20,21}. A statistical correlation between high-frequency components in the ground reaction force and the development of tendonitis in racehorses has also been shown²².

Control and damping of vibration is an important design feature of manmade mechanical systems. Machines are usually designed to be rigid, but elastic deformation is an essential functional property of the equine limb and some innovative legged robots²³. This elasticity and the multi-joint leg spring makes limb vibration inevitable, and it seems essential that this vibration is appropriately damped. The digital flexor muscles have extremely short fibres but a large physiological cross-sectional area. Muscles are good at absorbing energy²⁴, so these short-fibred muscles appear ideally arranged for absorbing energy during high-frequency small displacement vibration.

One front leg from each of six horses killed at an abattoir was mounted in a hydraulic press at three different limb orientations representing impact through to mid-stance. The limbs vibrated for

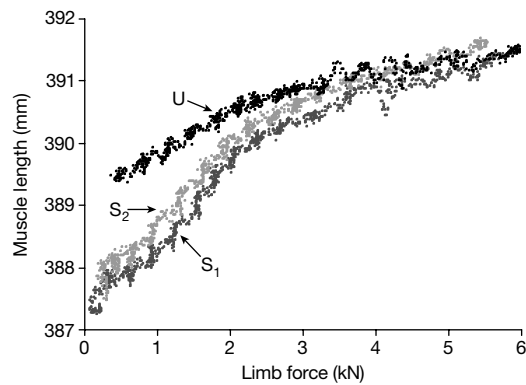


Figure 3 Relationship between limb force and muscle length for an equine superficial digital flexor muscle loaded *in situ* in the unstimulated state (U), and two sequential cycles with maximal electrical stimulation (S_1 , S_2). The difference between plots U and S_1 , S_2 represents the length change in the contracted muscle, and the difference between plots S_1 and S_2 represents the decline in contractile properties with repeated loading. Similar data were obtained for the deep digital flexor muscle.

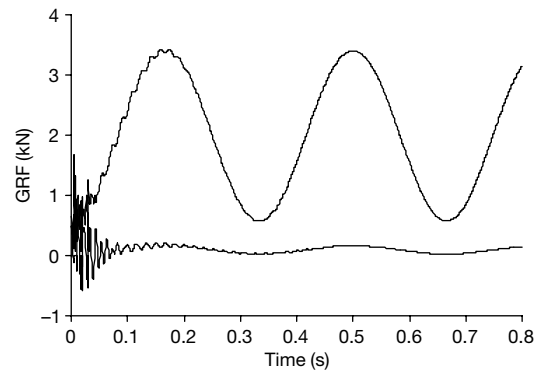


Figure 4 Vertical and horizontal ground reaction force (GRF) data produced from the equine limb model described in the text in the reference condition (leg vertical, no muscle activation, loading on tarmac). Top trace, vertical data; bottom trace, horizontal data. The initial oscillations are generated by the energy of the model being loaded by a mass of 200 kg. Two frequencies of oscillation are apparent at 2.9 and 57.5 Hz. There is no muscle stimulation in this case, and hence vibration damping is limited to the properties of the foot surface.

3–5 cycles at 25–45 Hz when an impulse was applied to the carpal joint with a 1-kg hammer. Vibration frequency increased with limb force (28 Hz at 1 kN to 38 Hz at 4 kN) and was 4 Hz higher at impact orientation (26.5° to vertical) than at mid-stance orientation. Another six legs were compressed up to 6 kN (roughly gallop force) at mid-stance orientation over 5 s, twice with and twice without electrical stimulation (50 Hz, 60 V) of the digital flexor muscles. It is unlikely that full muscle activation is achieved in this loading system (or during locomotion), but the length change would still be similar at low limb forces. Experiments were completed within 1 h of death, muscle temperature remained above 37 °C, and repeat plots were similar (Fig. 3).

At low limb forces, both muscles were 2–3 mm shorter when stimulated. The stimulated muscle lengthened more than the unstimulated muscle with increasing limb force (Fig. 3), absorbing energy in the limb force range at which the leg vibrations are damped (Fig. 2). The stimulated muscle lengthened more because the muscle was shorter at the start of loading, and when the isometric capacity of the contractile element was exceeded the muscle lengthened and the load was transferred to the parallel elastic element and the accessory ligament.

The accessory ligament is shorter (50 mm compared with 300 mm) and hence stiffer (N mm^{-1}) than the muscle aponeurosis, so at high elongations most of the force will pass through it. This load transfer from the compliant muscle to the stiff accessory ligament accounts for the plateau of both the active and the passive muscle length curves above a limb force of 3 kN. The accessory ligament therefore limits muscle length change, keeping the muscle fibres at an appropriate length for developing active force and hence absorbing energy during oscillation.

Muscle stimulation had minimal effect on the relationship between limb force and limb length, showing that there is minimal change in limb stiffness and thus little potential for limb tuning through contraction of the digital flexor muscles. The limb spring may, however, be tuned by the muscles associated with the elbow and shoulder joints or those attaching the scapula to the trunk.

We created a numerical model of the system that reproduced published *in vivo* joint angles and tendon strains (see Methods). The model in the reference state (leg vertical, no muscle activation and tarmac ground surface) also reproduced similar low (2.9 Hz) and high (57.5 Hz) natural frequencies to *in vivo* and *ex vivo* data when loaded with a mass of 200 kg, that is, half body mass (Fig. 4). Reducing vertical and horizontal surface stiffness by 500% from that representing tarmac ($k = 5 \times 10^5 \text{ N m}^{-1}$) to that representing

grass ($k = 1 \times 10^5 \text{ N m}^{-1}$) reduced the resonance frequencies by a much smaller amount to 2.7 and 34.1 Hz. This is due to the reduction in stiffness of the overall system. An increase in damping coefficient increased damping of vibration but did not change the frequency. The model was loaded at limb orientations of foot impact (26.5° to vertical) and mid-stance (vertical). At impact orientation, the resonance frequencies dropped from reference to 2.2 and 53.2 Hz because the limb is more compliant at this orientation.

In the model, muscle activation created muscle length changes greater than observed in the limb-loading experiment, had a damping effect on low-frequency oscillation (limb energy storage), but only a 3% tuning effect (2.9 to 3 Hz), which is less than the surface effect. There was, however, no damping or tuning effect on high-frequency limb vibration. This is because Hill muscle models (almost universal in biomechanical modelling) fail to simulate high-frequency energy absorption²⁴, because at high frequencies (and hence velocities) the contractile element remains almost isometric and the series elastic element absorbs most length change. Real muscles from a diverse range of animals (crayfish, frog, rat and rabbit), however, show a plateau or minimum in stiffness around 30–60 Hz (refs 24, 25). This effect is absent from muscle in rigor²⁵. This suggests that the minimum is an inherent property of cross-bridge dynamics²⁵, and we would predict that horse muscle will have similar frequency-dependent properties.

The cross-bridge model^{26,27} gives excellent simulations of the forces generated by live muscle fibres in response to small rapid length changes. We used the model to predict the energy absorbed by a cross-bridge when subjected to sinusoidal length changes of 0.5% at a range of frequencies. The assumption of constant displacement is reasonable because of the stiff accessory ligament in series with the muscle. There was a broad peak energy absorption of 15×10^{-21} J per cross-bridge per cycle centred around 100 Hz (Fig. 5), which is similar to that reported for real muscle^{24,25}. At 40 Hz, a single cross-bridge would absorb 12×10^{-21} J per cycle. Scaling-up for the digital flexor muscles (1 kg of muscle containing 0.3 mM myosin heads) gives a value of 2.5 J per cycle, which is sufficient to provide useful damping of limb vibration (energy 4–8 J), but is tiny compared with the energetic cost of locomotion². At stride frequency, the energy absorption was only 6×10^{-21} J per cross-bridge.

Muscle fibres will therefore absorb more vibrational energy around 30–100 Hz than predicted by the Hill model, in which stiffness increases monotonically with frequency. Experimentally

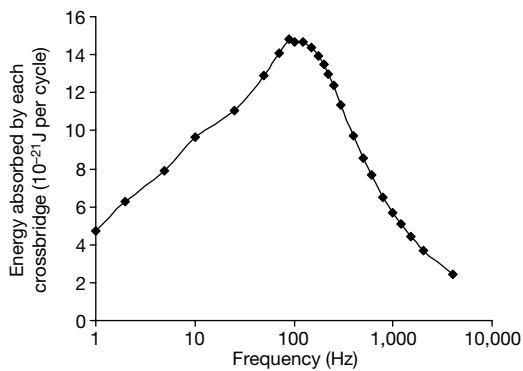


Figure 5 Plot of cycle work done on each cross-bridge in 10^{-21} J per cycle as a function of frequency (Hz) during a sinusoidal length change of 0.5%. These data were generated using the cross-bridge model of refs 26 and 27.

derived frequency-dependent muscle stiffness and phase data²⁵ were used to predict the impulse response of a muscle–tendon–mass system geared to represent the limb vibration mechanism. We found resonance at 30 Hz and 88% damping in the first 100 ms of the impulse response. This simple model shows a similar response to that predicted from the cross-bridge simulations and supports the hypothesis that the muscles have appropriate architecture and properties to damp vibrations in the frequency range that occur in the equine limb.

In summary, the apparently functionless but well-developed digital flexor muscles in the horse appear to act as dampers of high-frequency limb vibration rather than to flex the digit or tune the leg spring. A cross-bridge muscle model can reproduce this muscle energy absorption and should be useful in recreating this high-frequency damping in musculoskeletal models of impact attenuation. □

Methods

In vivo measurements

Eight horses were trotted over a forceplate (Kistler 9287BA) topped with either 6-mm-thick conveyor belt matting (a composite of polyester fibre and artificial rubber), bituminous roadstone (tarmac) or concrete. The frequency of leg vibration was determined from each plot of ground reaction force/time and averaged for six runs (three per forelimb) per horse and surface.

Measurements of muscle architecture

The superficial digital flexor muscle and the humeral (long-, intermediate- and short-fibred components separate), ulnar and radial heads of the deep digital flexor muscle were dissected free. We weighed each head and measured the fascial length (along the line of fibres between aponeuroses) at ten sites distributed across each muscle head. We calculated physiological cross-sectional area assuming a muscle density of 1.1 g cm^{-3} , and maximum isometric force assuming a capacity of 30 N cm^{-2} . No further correction for pennation angle or collagenous volume of the muscle was made.

Ex vivo limb loading

Forelimbs were cut perpendicular to the limb axis just proximal to the olecranon with the elbow at a mid-stance angle and a 13-mm diameter hole drilled through the distal humerus and the elbow joint. The leg was mounted in a hydraulic jig through a flat plate with a central, hinged 12-mm pin placed into the pre-drilled hole. The foot was placed on a force-measuring foot plate. We placed retroreflective markers over the centres of rotation of the elbow, carpal, metacarpophalangeal and distal interphalangeal joints. Retroreflective headed pins were inserted into the origin and muscle tendon junction of the deep and superficial digital flexor muscles, and data were recorded at 240 Hz (ProReflex, Qualisys). Wire electrodes (128-strand) were threaded through the deep and superficial digital flexor muscles, which were then wrapped in plastic film to prevent evaporative cooling.

Musculoskeletal model

A two-dimensional skeletal model of the equine forelimb was constructed, using five rigid-body segments connected by four ideal hinges. We used published segmental parameters (length, mass, moment of inertia and locations of the centre of mass)²⁸, and our model was conceptually similar to that in ref. 16. SD/FAST software (PTC) was used to obtain

equations of motion. The model was stabilized by two muscle–tendon units, the superficial and deep digital flexors, two passive tendinous structures, the suspensory ligament and accessory ligament of the deep digital flexor, and a linear torsion spring, the palmar carpal ligament. Muscles were represented by a three-component Hill model based on that in ref. 29. Passive elastic elements were represented by a quadratic force–length relationship. Ground contact forces F as a function of deformation x were applied at two points on the hoof using a visco-elastic model³⁰:

$$F = -k(x + b|\dot{x})$$

where $k = 5 \times 10^5$ or $1 \times 10^5 \text{ N m}^{-1}$, and $b = 0.5 \text{ s m}^{-1}$. Ground contact was modelled as a rigid hoof penetrating into a deformable surface. x is the penetration depth. The model coefficients were chosen such that this model accounts for the combined deformation of surface and hoof. The stiffness coefficient k for tarmac ($5 \times 10^5 \text{ N m}^{-1}$) is based on a peak ground reaction force of 5,000 N producing a static deformation of 1 cm; the equivalent deformation for turf ($k = 1 \times 10^5 \text{ N m}^{-1}$) is 5 cm. The damping coefficient b is based on ref. 30; $b = 0.5$ will produce a 50% increase in impact force when impact occurs at a speed of 1 m s^{-1} , when compared with static deformation.

Frequency domain model

The limb is represented by a one-dimensional muscle–tendon–mass system, representing the mechanism of limb vibration. With external force as the input and mass displacement as the output of the system, the transfer function $H(f)$ of this system in the frequency domain is:

$$H(f) = G \frac{k + s_f}{ks_f - 4(k + s_f)\pi^2 mf^2} \quad G = 3.0, k = 10^6 \text{ N m}^{-1}, m = 10 \text{ kg}$$

where f is the excitation frequency, k is tendon stiffness, and m is the oscillating mass, that is, the limb between the elbow and foot²⁸. G is the gear ratio for the limb, that is, the ratio between mass displacement and change in musculotendon length, derived from moment arms and bone lengths. The frequency-dependent stiffness s_f of the muscle, represented as a complex number with magnitude and phase, was taken from ref. 25 and scaled to a maximal force of 5,000 N and a fibre length of 5 mm. Four such muscle–tendon units were assumed to account for individual heads and accessory ligaments. Complex stiffness is the ratio between force and displacement when both are sinusoidal signals $e^{i\omega t}$ in the complex domain, where t is time and i is $\sqrt{-1}$. Stiffness is a complex number $S e^{i\phi}$ where ϕ is the phase difference between force and displacement and S is the amplitude ratio between force and displacement. The impulse response of the system was obtained by inverse Fourier transform of $H(f)$.

Received 1 March; accepted 12 October 2001.

- Dimery, N. J., Alexander, R. McN. & Ker, R. F. Elastic extension of leg tendons in the locomotion of horses (*Equus caballus*). *J. Zool.* **210**, 415–425 (1986).
- Minetti, A. E., Ardigo, L. P., Reinach, E. & Saibene, F. The relationship between mechanical work and energy expenditure of locomotion in horses. *J. Exp. Biol.* **202**, 2329–2338 (1999).
- Alexander, R. McN. & Bennet-Clark, H. C. Storage of elastic strain energy in muscle and other tissues. *Nature* **265**, 114–117 (1977).
- Alexander, R. McN. *Elastic Mechanisms in Animal Movement* (Cambridge Univ. Press, Cambridge, 1988).
- Biewener, A. A. & Roberts, T. J. Muscle and tendon contributions to force, work and elastic energy savings: a comparative perspective. *Exercise Sport Sci. Rev.* **28**, 99–107 (2000).
- Biewener, A. A. Muscle–tendon stresses and elastic energy storage during locomotion in the horse. *Comp. Biochem. Physiol. B* **120**, 73–87 (1998).
- Biewener, A. A., Konieczynski, D. D. & Baudinette, R. V. *In vivo* muscle force–length behaviour during steady state hopping in tammar wallabies. *J. Exp. Biol.* **201**, 1681–1694 (1998).
- Hof, A. L. *In vivo* measurement of the series elasticity release curve of human triceps surae muscle. *J. Biomech.* **31**, 793–800 (1998).
- Kurokawa, S., Fukunaga, T. & Fukashiro, S. Behaviour of fascicles and tendinous structures of human gastrocnemius during vertical jumping. *J. Appl. Physiol.* **90**, 1349–1358 (2001).
- Grandjean, J. Penniform muscles of the horses forelimb. *J. Anat. Abstr.* **132**, 318 (1981).
- Hermanson, J. W. & Cobb, M. A. Four forearm flexor muscles of the horse, *Equus caballus*: anatomy and histochemistry. *J. Morphol.* **212**, 269–280 (1992).
- Stephens, P. R., Nunamaker, D. M. & Butterweck, D. M. Application of a Hall effect transducer for the measurement of tendon strains in horses. *Am. J. Vet. Res.* **50**, 1089–1095 (1989).
- Herrick, W. C., Kingsbury, H. B. & Lou, D. Y. S. A study of the normal range of strain, strain rate and stiffness of tendon. *J. Biomed. Mat. Res.* **12**, 877–894 (1978).
- Bogert, A. J., van den Gerritsen, K. G. M. & Cole, G. K. Human muscle modeling from a user's perspective. *J. Electromyogr. Kinesiol.* **8**, 119–124 (1998).
- van Weeren, P. R., van den Bogert, A. J., Back, W., Bruin, G. & Barneveld, A. Kinematics of the standardbred trotter measured at 6, 7, 8 and 9 m s^{-1} on a treadmill after 5 months of prerace training. *Acta Anat.* **146**, 154–161 (1993).
- van den Bogert, A. J. & Schamhardt, H. C. Multi-body modelling and simulation of animal locomotion. *Acta Anat.* **146**, 95–102 (1993).
- Lake, M. J., Coyle, V. R. & Lees, A. High frequency characteristics of the lower limb during running. *Proc. 18th Congr. Int. Soc. Biomech.* (eds Müller, R., Gerber, H. & Stacoff, A.) 200–201 (Laboratory for Biomechanics, ETH Zurich, 2001).
- Carter, D. R. Mechanical loading histories and cortical bone remodeling. *Calcif. Tissue Int.* **36**(Suppl.), 19–24 (1984).
- Wang, X. T., Ker, R. F. & Alexander, R. McN. Fatigue rupture of wallaby tail tendons. *J. Exp. Biol.* **198**, 847–852 (1995).
- Cheney, J. A., Liou, S. Y. & Wheat, J. D. Cannon bone fracture in the thoroughbred racehorse. *Med. Bio. Eng. 11*, 613–620 (1973).

21. Nunamaker, D. M., Butterweck, D. M. & Provost, M. T. Fatigue fractures in thoroughbred racehorses: relationships with age, peak bone strain, and training. *J. Orthop. Res.* **8**, 604–611 (1990).
 22. Dow, S. M., Leendertz, J. A., Silver, I. A. & Goodship, A. E. Identification of subclinical tendon injury from ground reaction force analysis. *Equine Vet. J.* **23**, 266–272 (1991).
 23. Pratt, G. A. *et al.* Stiffness isn't everything. *Proc. 4th Int. Symp. Experimental Robotics, ISER, Stanford, California* 173–178 (1995).
 24. Ettema, G. J. C. & Huijting, P. A. Frequency response of rat gastrocnemius medialis in small amplitude vibrations. *J. Biomech.* **27**, 1015–1022 (1994).
 25. Kawai, M. & Brandt, P. W. Sinusoidal analysis: A high resolution method for correlating biochemical reactions with physiological processes in the activated skeletal muscles of rabbit, frog and crayfish. *J. Muscle Res. Cell. Motil.* **1**, 279–303 (1980).
 26. Piazzesi, G. & Lombardi, V. A cross-bridge model that is able to explain mechanical and energetic properties of shortening muscle. *Biophys J.* **68**, 1966–1979 (1995).
 27. Piazzesi, G. & Lombardi, V. Simulation of the rapid regeneration of the actin–myosin working stroke with a tight coupling model of muscle contraction. *J. Muscle Res. Cell. Motil.* **17**, 45–53 (1996).
 28. van den Bogert, A. J. *Computer Simulation of Locomotion in the Horse*. Thesis, Univ. Utrecht, The Netherlands (1989).
 29. van Soest, A. J. & Bobbert, M. F. The contribution of muscle properties in the control of explosive movements. *Biol. Cybern.* **69**, 195–204 (1993).
 30. Gerritsen, K. G. M., van den Bogert, A. J. & Nigg, B. M. Direct dynamics simulation of the impact phase in heel–toe running. *J. Biomech.* **28**, 661–668 (1995).

Acknowledgements

We acknowledge the assistance of R. C. Woledge in carrying out the cross-bridge model calculations and thank him for comments on the manuscript. We thank the Horserace Betting Levy Board, London, for funding this work.

Competing interests statement

The authors declare that they have no competing financial interests.

Correspondence and requests for materials should be addressed to A.M.W. (e-mail: awilson@rvc.ac.uk).

Maternal control of resting-egg production in *Daphnia*

Victor Alekseev* & Winfried Lampert

Max Planck Institute of Limnology, Department of Physiological Ecology, Postfach 165, D-24302 Ploen, Germany

Many planktonic organisms produce ‘resting’ stages when the environmental conditions deteriorate. Like seeds, resting stages can survive unfavourable conditions. The crustacean *Daphnia* normally reproduces by means of parthenogenetically produced normal, not resting, eggs—but occasionally switches to bisexual reproduction, which results in two resting eggs encased in a robust structure carried on the back of the female. This ‘ephippium’ is shed with the next moult, and can survive dormant for many years. The induction of resting-egg production requires multiple environmental stimuli, one of them being photoperiod^{1,2}. The switch from production of parthenogenetic eggs to resting eggs in *Daphnia* has recently been shown to be influenced by a maternal food effect³. Here we present evidence that female *Daphnia* transmit information not only about food but also on photoperiod to their offspring, and influence the production of resting eggs in the next generation. The combined maternal effects can be relevant for the correct timing of resting-egg production—for example, in discriminating between spring and autumn conditions.

After the work on calanoid copepod resting eggs that can survive for 300 years (ref. 4), studies on egg banks (analogous to seed banks)

focused on *Daphnia*^{5,6}. Understanding the dynamics of the egg bank requires information on the production and hatching of resting eggs. Ehippippia production in *Daphnia* displays a seasonal pattern. The induction of resting eggs has been long studied¹, but there is still no generally accepted theory about the causation of the seasonal pattern.

The switch in reproductive mode and the production of resting eggs require time, so it would be advantageous if the mother could anticipate the environmental conditions that her offspring will face. Growing interest in the control of phenotypic plasticity has resulted in consideration of the role of maternal effects⁷. In a variable environment, mothers can transmit information about environmental variability to the next generation, and influence the adaptive phenotypic response of their offspring⁸. For example, in *Daphnia*, such maternal effects have recently been reported for induced defences in response to predator-borne chemicals⁹. Maternal control of diapause has been reported for insects and mites⁷; the main factors in the maternal environment triggering the developmental switch in larvae are photoperiod and temperature¹⁰.

In *Daphnia*, bisexual reproduction and resting-egg formation is supposed to be induced by changing environmental conditions^{1,2} (that is, a phenotypic response) so individuals can alternate between modes of reproduction. Multiple environmental cues are required to induce resting-egg production, among them food availability, photoperiod and population density^{1,2}. Besides maternal nutrition³, another factor where transgenerational information can be expected is photoperiod, as the day length experienced by the mother and the day length experienced by succeeding generations can inform the offspring about the season in which they live¹⁰. With respect to the switch to resting-egg production, knowledge about the season is particularly important for *Daphnia*. As they are short-lived (one week from birth to maturation), measurements of the change in day length spread over two generations would be more reliable. Therefore, we raised *Daphnia pulex* in an experiment under all possible combinations of food conditions and photoperiod in the maternal and offspring generations, and measured the readiness of offspring to produce resting eggs (see Methods for details). Even at peak times of resting-egg production, only a few per cent of females in a natural population carry ehippippia^{11,12}. In order to increase the incidence of ehippippia in the experiments, we treated all offspring with a ‘shock’—a complex of diapause-inducing factors—as soon as they matured (see Methods).

None of the daphnid offspring produced resting eggs in a high-food environment. This is only partly consistent with recent experimental results³ that suggested that ehippippia production in *Daphnia* requires an asymmetrical mismatch in food conditions between mother and offspring: that is, a ‘step-down’ change in food. Using multiple cues, we could induce resting eggs when both mother and offspring lived at low food conditions, but never with

Table 1 Effect of environment on resting-egg production

Maternal environment	Offspring environment			
	High food		Low food	
	SD	LD	SD	LD
High food				
SD	0	0	52.3 (7.4)	38.0 (14.7)
LD	0	0	13.0 (7.2)	11.0 (11.0)
Low food				
SD	0	0	7.5 (7.5)	15.8 (4.6)
LD	0	0	0	30.7 (15.2)

Effect of maternal and offspring environment on the mean (±s.e.) percentage of daphnids producing resting eggs (ephippippia) within two clutches after the environmental shock (see Methods). Females and offspring experienced either high (1 mg C l⁻¹) or low (0.2 mg C l⁻¹) food concentrations in combination with short (10 h light; SD) or long (16 h light; LD) photoperiod. Kruskal–Wallis ANOVA by ranks yielded a highly significant effect of offspring food concentration ($H = 22.3$, $n = 48$, $P < 0.0001$). Pairwise comparisons (Kruskal–Wallis test) within the offspring low-food treatments yield significant effects of mother’s photoperiod for the maternal high-food treatments ($H = 5.85$, $n = 12$, $P = 0.016$) and of offspring photoperiod for the maternal low-food treatments ($H = 6.22$, $n = 12$, $P = 0.013$).

* Present address: Zoological Institute of the Russian Academy of Sciences, St Petersburg, 199034, Russia.